

## Thermal Boundary Resistance in GaN Films Measured by Time Domain Thermoreflectance with Robust Monte Carlo Uncertainty Estimation

Thomas L. Bougher, Luke Yates, Chien-Fong Lo, Wayne Johnson, Samuel Graham & Baratunde A. Cola

To cite this article: Thomas L. Bougher, Luke Yates, Chien-Fong Lo, Wayne Johnson, Samuel Graham & Baratunde A. Cola (2016) Thermal Boundary Resistance in GaN Films Measured by Time Domain Thermoreflectance with Robust Monte Carlo Uncertainty Estimation, *Nanoscale and Microscale Thermophysical Engineering*, 20:1, 22-32, DOI: [10.1080/15567265.2016.1154630](https://doi.org/10.1080/15567265.2016.1154630)

To link to this article: <http://dx.doi.org/10.1080/15567265.2016.1154630>

 View supplementary material [↗](#)

 Accepted author version posted online: 22 Mar 2016.  
Published online: 22 Mar 2016.

 Submit your article to this journal [↗](#)

 Article views: 45

 View related articles [↗](#)

 View Crossmark data [↗](#)



# Thermal Boundary Resistance in GaN Films Measured by Time Domain Thermoreflectance with Robust Monte Carlo Uncertainty Estimation

Thomas L. Bougher<sup>a</sup>, Luke Yates<sup>a</sup>, Chien-Fong Lo<sup>b</sup>, Wayne Johnson<sup>b</sup>, Samuel Graham<sup>c</sup>, and Baratunde A. Cola<sup>c</sup>

<sup>a</sup>George W. Woodruff School of Mechanical Engineering and Heat Lab, Georgia Institute of Technology, Atlanta, Georgia, USA; <sup>b</sup>IQE, Taunton, Massachusetts, USA; <sup>c</sup>George W. Woodruff School of Mechanical Engineering; School of Material Science and Engineering; and Heat Lab, Georgia Institute of Technology, Atlanta, Georgia, USA

## ABSTRACT

In this work, we investigate the thermal boundary resistance and thermal conductivity of GaN layers grown on Si with 100 nm AlN transition layers using time domain thermoreflectance (TDTR). The GaN layers ranged from 0.31 to 1.27  $\mu\text{m}$ . Due to the challenges in determining the thermal boundary resistance of the buried interfaces found in this architecture, a new data reduction scheme for TDTR that utilizes a Monte Carlo fitting method is introduced and found to dramatically reduce the uncertainty in certain model parameters. The results show that the GaN thermal conductivity does not change significantly with layer thickness, whereas the resistance of the AlN layer decreases slightly with GaN thickness.

## ARTICLE HISTORY

Received December 23, 2015

## KEYWORDS

Gallium nitride

## Introduction

Wide bandgap semiconductors based on AlGaIn/GaN heterojunctions are of technological importance to the development of future high-power and high-frequency radio frequency and power electronics applications. Due to the lack of a sufficient supply of lattice-matched substrates, these devices are often grown on nonnative substrates (e.g., sapphire, Si, and SiC) with the use of extensive engineering of the interface in order to relax stresses in the GaN and reduce the number of defects that are directly related to the quality, performance, and lifetime of the devices [1]. This interface engineering is accomplished by the growth of a single or multiple buffer layers often composed of aluminum nitride (AlN) but may also consist of more complex structures, such as superlattices (SLs) of AlN/GaN or AlN/AlGaIn. These transition layers have been shown to add large thermal resistances to the structure [2], which will lead to a higher junction temperature for a given power density. To this end, methods to accurately assess the thermal properties of the GaN layers and the buried interfaces created between the GaN and growth substrate are very important in order to provide feedback to the growth process and optimize the device structures.

In this work, we explore the impact of the use of AlN and SL transition layers on the thermal boundary resistance (TBR) in GaN heterostructures grown on <111>Si wafers. Time-domain thermoreflectance (TDTR) measurements are used to estimate the TBR on each device stack with increasing complexity beginning with samples of AlN or SL on Si and then samples of GaN/AlN/Si or GaN/SL/Si. Through the use of a Monte Carlo technique for uncertainty estimation we are able to

**CONTACT** Baratunde A. Cola ✉ [cola@gatech.edu](mailto:cola@gatech.edu) ☎ Georgia Institute of Technology, 345 Ferst Dr. NW, Atlanta, GA 30313; Samuel Graham ✉ [sgraham@gatech.edu](mailto:sgraham@gatech.edu) ☎ 771 Ferst Dr. NW, Atlanta, GA, 30313.

Color versions of one or more of the figures in this article can be found online at <https://www.tandfonline.com/umte>.

Supplemental data for this article can be accessed on the publisher's website

extract the resistance of the AlN transition layer separate from the GaN layer and Al-GaN boundary resistance.

## Experimental methods

In this work we study gallium nitride thin films grown epitaxially on  $\langle 111 \rangle$ Si wafers. Because of the large lattice mismatch between GaN and Si [3, 4], an aluminum nitride buffer layer (100 nm) is grown on top of the Si to allow for uniform growth and relax the stress in the GaN layer. The GaN and AlN layers were grown using metal organic chemical vapor deposition (MOCVD). GaN thickness of 0.31, 0.50, 0.62, 0.84, and 1.27  $\mu\text{m}$  were tested (Figure 1); in addition, a 0.87- $\mu\text{m}$  GaN layer on top of a 0.85- $\mu\text{m}$  superlattice that consists of 35 alternating layers of GaN (20 nm)/AlN(4 nm) was tested. Underneath the superlattice is 50-nm  $\text{Al}_x\text{Ga}_{(1-x)}\text{N}$  and then 100 nm of AlN on top of the Si substrate. Two samples were tested without GaN layers to measure the properties of the underlying materials: (1) 100 nm of AlN on Si and (2) 0.78  $\mu\text{m}$  SL, 50 nm AlGaIn, 100 nm AlN on Si. All samples were coated with a layer of Al for the TDTR measurement, nominally 90 nm, with the exact thicknesses measured by picosecond acoustics [5] (Figure 2b, inset).

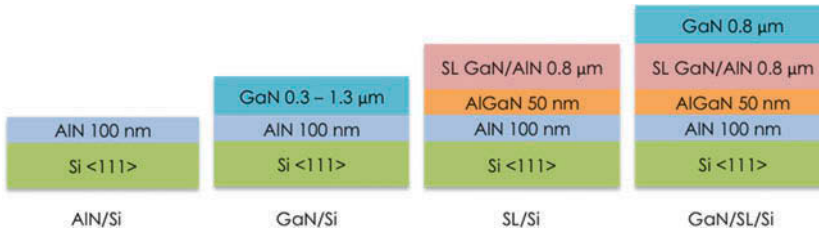


**Figure 1.** Sample configurations tested in this study. All samples are grown via MOCVD on Si  $\langle 111 \rangle$  substrate. Superlattice (SL) consists of 35 alternating layers of GaN (20 nm) and AlN (4 nm). Nominal sample thicknesses are shown.

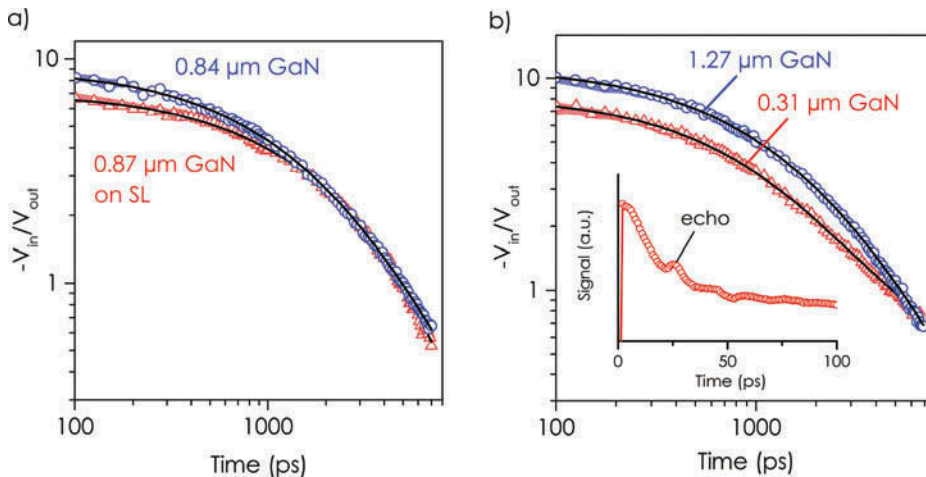


**Figure 2.** TDTR data for various samples. (a) Comparison of the thinnest and thickest GaN layers on AlN/Si, 0.31- and 1.27- $\mu\text{m}$ -thick GaN. (b) Comparison of  $\sim 0.8$ - $\mu\text{m}$  GaN with and without 0.84- $\mu\text{m}$  SL underneath the GaN layer. Symbols represent experimental data and lines represent theoretical best fits. The shaded area behind each data set represents plus and minus one standard deviation of the measured ratio, which is typically narrower than the data markers. Inset: representative acoustic echo for 1.27- $\mu\text{m}$  GaN sample.

We measured the thermal properties of multilayer GaN samples at room temperature using TDTR, a well-established technique to measure the thermal conductivity and thermal boundary resistance of thin films. The experimental details of TDTR have been explained thoroughly elsewhere [6–8], but, briefly, TDTR is a pump and probe technique that utilizes an ultrafast laser with a pulse width of less than 1 ps to thermally excite a sample, measure the temperature decay, and extract thermal properties using a diffusive heat conduction model over timescales from 100 to 7,000 ps. In our implementation of TDTR we use a Ti:sapphire laser oscillating at 80 MHz with an energy of  $\sim 40$  nJ/pulse (3W average power) at a wavelength of 800 nm. An electro-optic modulator chops the pump pulse at a frequency between 0.5 and 12 MHz (6.3 MHz in this work) and the pump pulse is frequency doubled to 400 nm in a BiBO crystal. The probe beam is expanded prior to entering the double-pass delay stage to minimize variation in spot size with delay time [9] and compressed again prior to focusing onto the sample. The pump and probe beams impinge on the transducers concentrically at a normal angle; in this work we use a  $1/e^2$  beam diameter of 70  $\mu\text{m}$  for the pulse and 25  $\mu\text{m}$  for the probe with a power of 50 mW and 10 mW for the pump and probe, respectively. The model accounting for radial conduction is used [7], although for the beam sizes used the conduction is primarily one-dimensional. We have confirmed the system with fused quartz and monocrystalline Si and found values similar to those reported in literature ( $1.32 \pm 0.09$  W/m-K for quartz and  $147 \pm 14$  W/m-K for Si).

The sensitivity for TDTR measurements is defined as

$$S_p = \frac{d(\ln R)}{d(\ln p)} = \frac{dR/R}{dp/p}, \quad (1)$$

where  $R$  is the measured ratio of in phase temperature signal to out of phase temperature signal ( $-V_{\text{in}}/V_{\text{out}}$ ) and  $p$  is the value of the property of interest [10, 11]. The sensitivity to the GaN thermal conductivity increases linearly with GaN thickness over the values tested in this work. For a 0.3- $\mu\text{m}$  GaN layer the sensitivity is below 0.1, making it difficult to extract an accurate value for thermal conductivity; in contrast, the sensitivity at 1.27  $\mu\text{m}$  is approximately 0.3, making it possible to report the GaN thermal conductivity.

In our GaN samples there are five unknowns, including two-layer thermal conductivity values ( $k_{\text{GaN}}$ ,  $k_{\text{AlN}}$ ) and three boundary resistance values ( $R_{\text{Al-GaN}}$ ,  $R_{\text{GaN-AlN}}$ ,  $R_{\text{AlN-Si}}$ ). The sensitivity to the two buried boundary resistances ( $R_{\text{GaN-AlN}}$  and  $R_{\text{AlN-Si}}$ ) and thermal conductivity of the 100-nm AlN layer are very low and not unique at the modulation frequency used in this work (6.3 MHz). We do find, however, that the resulting values for the effective AlN resistance ( $R_{\text{AlN,eff}}$ ) are different depending on how this resistance is treated in data fitting. The equation for the  $R_{\text{AlN,eff}}$  is

$$R_{\text{AlN,eff}} = \text{TBR}_{\text{GaN-AlN}} + (L/k)_{\text{AlN}} + \text{TBR}_{\text{AlN-Si}}, \quad (2)$$

where  $\text{TBR}_{x-y}$  is the thermal boundary resistance between layers  $x$  and  $y$ ,  $L$  is the layer thickness, and  $k$  is the layer thermal conductivity. We fit the same data with the  $R_{\text{AlN,eff}}$  treated three separate ways: as just a layer (all resistance from TBR is included in the AlN layer resistance), as just an interface (there is no heat capacity of a layer, just a total TBR), and as a layer with two interfaces (the actual scenario). We find different resulting values for  $R_{\text{AlN,eff}}$  in each case with the best fits obtained for the most realistic case where there is an AlN layer and an interface on each side. The resulting fitted values of the two interfaces and the layer thermal resistance have no meaning individually (because the sensitivity to each is low and not unique), but we sum them to calculate  $R_{\text{AlN,eff}}$ . To verify the assumption that the fit is sensitive to this total effective resistance and not individual parameters, we perform a number of fits where one of the three parameters is held constant over a range of values (a total of 100 permutations). We observe that the best-fit values for the other parameters shift to maintain a similar total resistance for each

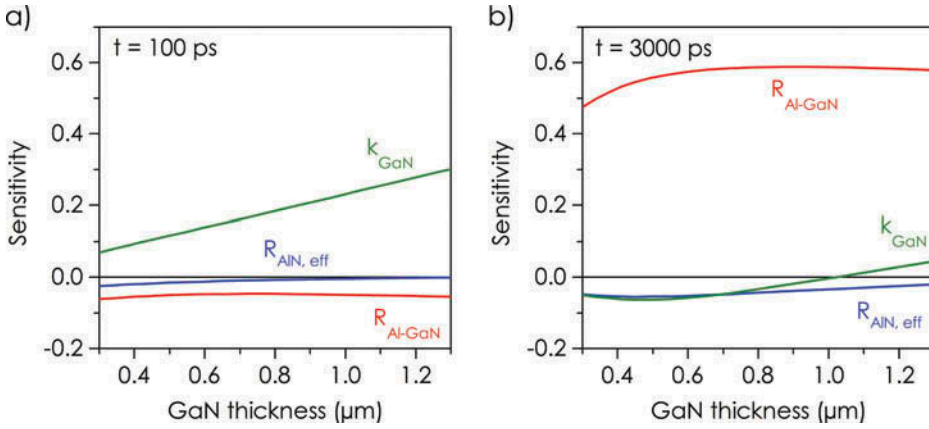


**Figure 3.** Sensitivity to boundary resistance and thermal conductivity as a function of GaN layer thickness at 6.3 MHz for GaN/Si sample. (a) Delay time of 100 ps. (b) Delay time of 3000 ps. The two boundary resistances and layer thermal conductivity for AlN have been combined into a single value,  $R_{\text{AlN,eff}}$ .

permutation. This is similar to the observation that the phase response in the photoacoustic technique can be sensitive only to the total resistance of a set of layers and not the individual components [12]. The sensitivity to each unknown parameter is shown in Figure 3 as a function of GaN layer thickness (for GaN/Si samples) at two different delay times.

An expression for uncertainty in TDTR is given by Wei et al. [13]:

$$\left(\frac{\delta_p}{p}\right)^2 = \left(R \cdot \frac{\delta_\phi}{S_p}\right)^2 + \sum \left(\frac{S_\alpha}{S_C} \cdot \frac{\delta_\alpha}{\alpha}\right)^2, \quad (3)$$

where  $\delta_p$  is the uncertainty to the parameter of interest,  $p$ ,  $\delta_\phi$  is the uncertainty in determining the zero delay position,  $\delta_\alpha$  is the uncertainty to parameter  $\alpha$ ,  $S$  is sensitivity, and  $R$  is the ratio signal measured ( $-V_{\text{in}}/V_{\text{out}}$ ). The second term is the standard expression for uncertainty using partial derivatives and is valid when the uncertainties are small and Gaussian, but for parameters with sensitivity below 0.2 the reported uncertainty values tend to increase rapidly, often exceeding 100%. Though it is always preferable to modify the sample configuration to improve the sensitivity of a parameter of interest, this may not always be possible. In our case we wish to measure the boundary resistance at buried interfaces for realistic device stacks; there is no simple way to modify the samples to increase the sensitivity; therefore, we propose an alternative method to determine the uncertainty in TDTR parameters. Using a Monte Carlo simulation is a method to estimate uncertainties in cases where sensitivity may be low or uncertainties may be partially correlated. Recently a Monte Carlo technique was used to calculate the error associated with 3-omega measurements of supported graphene [14] and the error using a modified reference bar technique [15].

Implementation of the Monte Carlo technique for uncertainty estimation is straightforward but computationally expensive due to the large number of iterations necessary to ensure that the statistics have stabilized. The main advantage of the Monte Carlo method over analytical expressions in uncertainty estimation is that it requires no prior knowledge of how errors affect the uncertainty and how different errors may interact [16]. The main sources of uncertainty in TDTR are the noise in the in-phase ( $V_{\text{in}}$ ) and out-of-phase measurements ( $V_{\text{out}}$ ) by the lock-in amplifier and the error in estimating the known properties in the thermal model [13]. To estimate the uncertainty in the lock-in amplifier measurement we take 20 measurements at each delay time to generate a mean and standard deviation of the lock-in amplifier ratio ( $-V_{\text{in}}/V_{\text{out}}$ ). The uncertainty of individual parameters is discussed in the Supplementary Information.

We assume that all errors are normally distributed and sample randomly from a normal distribution to create a new data set and a new set of given model properties based on the mean and standard deviation of the inputs. In each iteration this unique data set and set of model parameters is used to fit the unknown properties, and the process is repeated 1,000 times to generate a distribution of possible outcomes for each unknown parameter (Supplementary Information). Verification of the technique was conducted by comparing the uncertainty in measuring the thermal conductivity of bulk monocrystalline Si ( $k_{\text{Si}}$ ) and the thermal boundary resistance between Si and the Al transducer. In this scenario, both unknown parameters have an absolute peak sensitivity of  $\sim 0.5$ , so the Monte Carlo technique and the analytical expression should be in good agreement. The Monte Carlo simulation reports  $k_{\text{Si}} = 147.4 \text{ W/m-K} +13.0/-12.2\%$  based upon a 90th/10th percentile confidence interval compared with the analytical expression, which predicts  $\pm 9.9\%$ . It is expected that the Monte Carlo simulation would report slightly higher uncertainties because this takes into account the noise in the signal for each data point, not just the zero crossing. When considering only the model parameters' uncertainty in both techniques, the Monte Carlo simulation reports a 90/10 confidence interval of  $+9.6/-9.8\%$  compared to  $9.3\%$  for the analytical expression.

## Results and discussion

The thermal conductivity of the (AlN) 4 nm to (GaN) 18 nm SL was found to be  $7.0 +0.8/-0.7 \text{ W/m-K}$ , which is slightly lower than the value of  $\sim 10 \text{ W/m-K}$  observed by Koh et al. for a similar composition AlN-GaN SL [17]. The AlN-GaN SL in this prior work are grown by radio frequency molecular beam epitaxy (MBE) and are between 200 to 500 nm in thickness, and the SL in this work is grown by MOCVD with a total thickness of 780 nm (35 periods). This is a total layer resistance of  $112 \text{ m}^2\text{-K/GW}$ , which is substantially larger than the resistance of the GaN on AlN samples. The total resistance of the GaN on SL sample was  $120.4 \text{ m}^2\text{-K/GW}$  compared to  $12.2 +2.2/-2.0 \text{ m}^2\text{-K/GW}$  for GaN on AlN. Any desire to relax the GaN layer through a superlattice structure would have to consider the adverse effects of the increase in the GaN-to-substrate total thermal resistance by a factor of 10.

The thermal conductivity of intrinsic single-crystal AlN is over  $200 \text{ W/m-K}$  [18]; however, thin defective films used in transition layers are often an order of magnitude lower [19]. It was not possible to extract the AlN layer thermal conductivity from the Al/AlN/Si sample because the layer was only 100 nm thick and fitting results indicate that the layer resistance was relatively low. The combined resistance of the AlN layer and AlN-Si interface was  $5.3 +3.0/-2.7 \text{ m}^2\text{-K/GW}$ . We had initially planned to use the AlN-Si sample to measure the AlN thermal conductivity and AlN-Si interface to input into the GaN/AlN/Si samples, but given the low resistance, it is not possible to separate these values and thus there is no way to compare to the AlN effective resistance of the GaN samples, which also includes the GaN-AlN TBR. The fifth percentile of the AlN thermal conductivity was  $25 \text{ W/m-K}$ , indicating that the true value is likely no less than this value, which is higher than many reported values in literature using MBE [20] and sputtering [21], although we find no previous measurements for AlN grown by MOCVD. Previous studies have estimated the thermal conductivity of highly dislocated AlN of similar thickness to be  $47 \text{ W/m-K}$  based on the Born-Von-Karman Slack model [22].

The TBR between Al-GaN varied from  $6.3$  to  $8.3 \text{ m}^2\text{-K/GW}$ , which is slightly lower than the values reported by Donovan et al., who reported  $\sim 12 \text{ m}^2\text{-K/GW}$  [23]. Both our values and those of Donovan et al. [23] are within the range observed by Cho et al. for GaN/AlN/Si samples ( $6.2-17.6 \text{ m}^2\text{-K/GW}$ ) [24]. The resistance between the Al transducer and the GaN will depend heavily upon the specifics of the metal deposition as well as the cleanliness of the GaN prior to deposition, so it is unsurprising that the reported boundary resistance varies somewhat.

### Total thermal resistance and GaN thermal conductivity

Representative TDTR scans for different samples are shown in Figure 2. Figure 2a shows a comparison of similar GaN layers on AlN/Si and on SL/AlGaN/AlN/Si, and Figure 2b shows a comparison between the thinnest and thickest GaN layers measured on AlN/Si (0.31  $\mu\text{m}$  versus 1.27  $\mu\text{m}$ ).

The total resistance of the sample is considered as follows:

$$R_{\text{total}} = \left(\frac{L}{k}\right)_{\text{GaN}} + TBR_{\text{GaN-AlN}} + \left(\frac{L}{k}\right)_{\text{AlN}} + TBR_{\text{AlN-Si}} = \left(\frac{L}{k}\right)_{\text{GaN}} + R_{\text{AlN,eff}}, \quad (4)$$

where  $L$  is a layer thickness,  $k$  is thermal conductivity, and  $TBR_{x-y}$  is a thermal boundary resistance between layers  $x$  and  $y$ . The layer and boundary resistance of the Al layer ( $R_{\text{GaN-Al}}$ ) are not considered in the total resistance because the Al layer is added only to facilitate the TDTR measurement and not an inherent part of the material stack. Because the sensitivity to  $R_{\text{GaN-Al}}$  is high (Figure 3b) at different time delays compared to the sensitivity to the GaN layer, it is possible to accurately extract the Al boundary resistance separate from the other parameters of interest [25]. From the slope of the line, the constant GaN thermal conductivity would be 161 W/m-K with an  $R^2$  of 0.88. However, this value of thermal conductivity is inconsistent with the fitted thermal conductivity at 0.84 and 1.27  $\mu\text{m}$  (127 +28/-20 W/m-K and 136 +19/-14 W/m-K, respectively). The effective resistance of the AlN transition layer ( $R_{\text{AlN,eff}}$ ) appears to have a slight dependence upon GaN thickness (Figure 4b); when this resistance is removed from the total resistance the remaining resistance is the GaN layer resistance ( $R_{\text{GaN}}$ ). The GaN resistance has a good linear dependence on thickness ( $R^2 = 0.97$ ) with an intercept nearly passing through zero (-0.0022  $\text{m}^2\text{-K/GW}$ ). The slope of this line estimates the average GaN thermal conductivity to be 128 W/m-K, which is consistent with the fitted values for the 0.8- and 1.27- $\mu\text{m}$  GaN samples. This implies that the GaN thermal conductivity is not a strong function of layer thickness over the range tested here, which is the same conclusion made in other similar work [24] and would be the case when the reduction in thermal conductivity due to defect density dominates over boundary scattering. Luo et al. reported that for an  $\sim 5\text{-}\mu\text{m}$  GaN film grown via lateral epitaxial overgrowth MOCVD the thermal conductivity is greater than 155 W/m-K, whereas a 50- $\mu\text{m}$  film grown via hydride vapor phase epitaxy had a thermal conductivity similar to that observed in this work (135 W/m-K) [26]. The range of 127 to 136 W/m-K is about a factor of two lower than reports for bulk single-crystal GaN [18, 27]. This is also somewhat lower than that recently reported for MBE GaN of similar thickness on AlN/Si (185  $\pm$  20 W/m-K) and GaN on AlN/SiC (167  $\pm$  15 W/m-K) [24], although this GaN was grown via MBE rather than MOCVD. Recent measurements on MOCVD GaN (150 W/

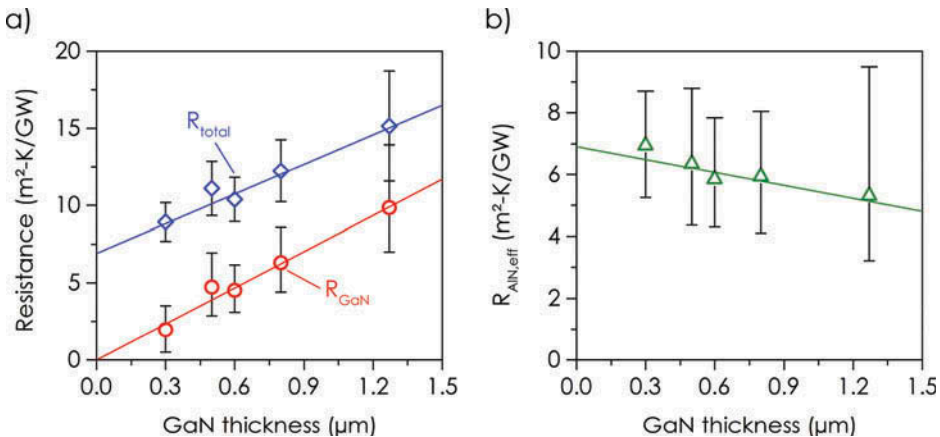


**Figure 4.** Resistance as a function of GaN layer thickness. (a) Total sample resistance ( $R_{\text{total}}$ ) and  $R_{\text{total}} - R_{\text{AlN}}$  (effective AlN resistance) as a function of GaN thickness for samples with 100-nm AlN transition layer on Si.  $R_{\text{total}}$  does not include  $R_{\text{Al-GaN}}$ . (b) AlN effective resistance as a function of GaN layer thickness for samples with 100-nm AlN transition layer on Si.

**Table 1.** GaN layer properties.

GaN thickness <sup>a</sup> (μm)	Transition layer <sup>b</sup>	Thermal conductivity (W/m-K) <sup>c</sup>			TBR <sub>eff</sub> (m <sup>2</sup> -K/GW) <sup>d</sup>		
		50th	10th	90th	50th	10th	90th
0.308	AlN	—	—	—	7.0	5.3	8.7
0.500	AlN	—	—	—	6.4	4.4	8.8
0.620	AlN	—	—	—	5.9	4.3	7.8
0.840	AlN	127	107	155	5.9	4.1	8.1
1.273	AlN	136	122	155	5.3	3.2	9.5
0.874	SL/AlGaIn/AlN	104	75	184	120	108	133

<sup>a</sup>GaN layer thickness measured by in situ reflectivity with 5% uncertainty and confirmed with TEM.

<sup>b</sup>AlN transition layer is 100 nm, AlGaIn is 50 nm, and SL GaN(20 nm)/AlN(4 nm) is 0.84 μm. All samples are on Si(111).

<sup>c</sup>Reported GaN thermal conductivity values are from Monte Carlo simulation; 50th, 10th, and 90th are percentiles of 1,000 fits varying model parameters and experimental data according to their uncertainty. Each reported value is the average of three different measurements.

<sup>d</sup>TBR<sub>eff</sub> calculated based on Eq. (2) for  $R_{\text{AlN,eff}}$  for AlN transition layer. For the SL/AlGaIn/AlN layer only the layer resistance of the SL is reported because the other components are difficult to measure accurately and only comprise ~10% of the total value.

**Table 2.** Thermal properties of GaN films from literature.

Study	GaN thickness (μm)	Substrate	Growth	GaN thermal conductivity (W/m-K)	GaN/sub TBR (m <sup>2</sup> -K/GW)	Al/GaN TBR (m <sup>2</sup> -K/GW)
This work	—	Si	MOCVD	127–136	5.3–7.0	6.3–8.3
Cho et al. [24]	0.5–1.7	Si	MBE	185	7.8	6.2–17.6
Cho et al. [24]	0.6–1.6	SiC	MBE	167	5.3	—
Sarua et al. [28]	1.2	Si & SiC	MOCVD	150	33	—
Luo et al. [26]	5	Al <sub>2</sub> O <sub>3</sub>	Lateral epitaxial overgrowth	>155	—	—
Manoi et al. [30]	—	SiC	MOCVD	—	15–50	—
Donavan et al. [23]	3	Al <sub>2</sub> O <sub>3</sub>	—	—	—	~12

m-K [28]) have shown lower thermal conductivity values than MBE GaN but still slightly higher than the values observed in this work, which could be a result of a higher defect density. A summary of thermal conductivity and boundary resistance values from previous GaN studies is shown in Table 2.

The thermal conductivity of the GaN on SL cannot be determined as accurately as the GaN on AlN/Si, due to reduced sensitivity resulting from the SL layer beneath the GaN and due to the propagation of uncertainty from the SL thermal conductivity that was measured in a separate sample. Despite the high uncertainty, it is possible to discern that the thermal conductivity of the GaN on SL is lower than GaN on AlN/Si for the same thickness (Table 1). The GaN on SL has higher C content for creating semi-insulating layers for power electronic devices, which is likely reducing the thermal conductivity.

The resistance of the GaN layer varied between 2.0 and 9.8 m<sup>2</sup>-K/GW, which is comparable to the resistance of the AlN transition layer. The total resistance of the sample ( $R_{\text{GaN}} + R_{\text{AlN,eff}}$ ) was between 8.9 and 15.2 m<sup>2</sup>-K/GW (Figure 4a); in comparison this represents the same thermal resistance as only 1.3 to 2.2 μm of the Si substrate. In this material stack it is likely that the bottleneck to heat dissipation is the relatively low thermal conductivity of the Si substrate (~140 W/m-K) compared to SiC (~420 W/m-K) [28].

### Effective resistance of AlN transition layer

The effective AlN layer resistance varied from 7.0 +1.8/–1.7 m<sup>2</sup>-K/GW for the thinnest GaN sample to 5.3 +4.2/–2.1 m<sup>2</sup>-K/GW for the thickest GaN sample (Figure 4b). Although the uncertainty of  $R_{\text{AlN,eff}}$  is high, the resistance exhibited a trend of decreasing with increasing GaN thickness. This change in resistance of the transition layer could be due to changes in residual stress of the samples;

photoluminescence measurements (supplementary information) show a strong increase in tensile stress at the surface of the GaN layer as the thickness increases. Recent simulation work has demonstrated that the interface conductance will increase when the stiffness of one of the layers at an interface is increased [29], which is consistent with the trend observed here where the samples with higher tensile stress exhibit a higher interface conductance. Another possible explanation for this trend is that the phonon density of states in the GaN layer is changing with thickness, although in this case one would expect to see changes in the GaN thermal conductivity, which are not observed here. The measured effective AlN resistance is comparable to the previous  $R_{\text{AlN,eff}}$  measured with TDTR of  $7.8 \pm 1.2 \text{ m}^2\text{-K/GW}$  for GaN/AlN/Si, although the AlN layer was only 38 nm compared to 100 nm in this work. In this prior work the layers were grown by MBE, compared to MOCVD in this work. The TBR for GaN/AlN/SiC samples have been reported to be  $5.3 \pm 1.3 \text{ m}^2\text{-K/GW}$  using TDTR [24] and  $5.1 \pm 2.8 \text{ m}^2\text{-K/GW}$  for AlN/SiC using 3-omega [22]. Manoi et al. measured a wide range of samples with SiC substrates with Raman thermography varying from 15 to  $50 \text{ m}^2\text{-K/GW}$  at  $150^\circ\text{C}$  [30].

### Uncertainty in GaN data

The confidence bounds for the GaN-Al TBR are nearly identical using the Monte Carlo simulation or the analytical equation (Figure 5) because the sensitivity to the parameter is high for all GaN thicknesses (Figure 3b). However, the analytical equation overpredicts the uncertainty by a large degree for  $R_{\text{AlN,eff}}$  (Figure 5b). For GaN layers thicker than  $0.5 \mu\text{m}$  the analytical equation predicts an uncertainty greater than 100%. The uncertainty for  $R_{\text{AlN,eff}}$  generally increases as the GaN layer thickness increases and the AlN layer is buried farther away from the transducer layer due to a reduced sensitivity to the resistance in the TDTR model.

As the uncertainty becomes larger the probability distribution becomes wider; in Figure 6 the median value for thermal conductivity is similar for both  $0.6$  and  $1.3 \mu\text{m}$ ; however, the  $0.6 \mu\text{m}$  distribution is much wider compared to the  $1.3\text{-}\mu\text{m}$  sample. The opposite is true for the  $R_{\text{AlN,eff}}$  distribution, where it is much narrower for the thinner sample (Figure 6b). The two histograms in Figure 6 demonstrate clearly that even a small difference in the thickness of the GaN layer changes what parameters can accurately be measured using TDTR. The thermal conductivity of the  $1.3\text{-}\mu\text{m}$  GaN layer can be reported with less than 15% uncertainty and the 90th percentile for the  $0.6 \mu\text{m}$  is almost 200%, indicating that this value cannot be properly measured. In contrast, the effective AlN resistance in the  $0.6\text{-}\mu\text{m}$  GaN sample can be measured

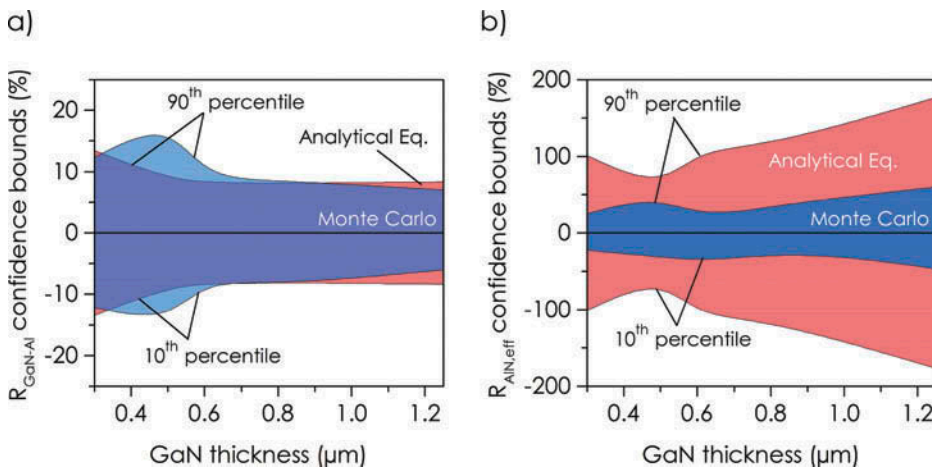


**Figure 5.** Confidence bounds from Monte Carlo simulation and analytical equation. Confidence bounds:  $90^{\text{th}} = 100 * (R_{90^{\text{th}}} - R_{50^{\text{th}}})/R_{50^{\text{th}}}$ ,  $10^{\text{th}} = 100 * (R_{10^{\text{th}}} - R_{50^{\text{th}}})/R_{50^{\text{th}}}$ . (a) Effective AlN resistance ( $R_{\text{AlN,eff}}$ ). (b) Thermal boundary resistance between Al and GaN ( $R_{\text{GaN-Al}}$ ).

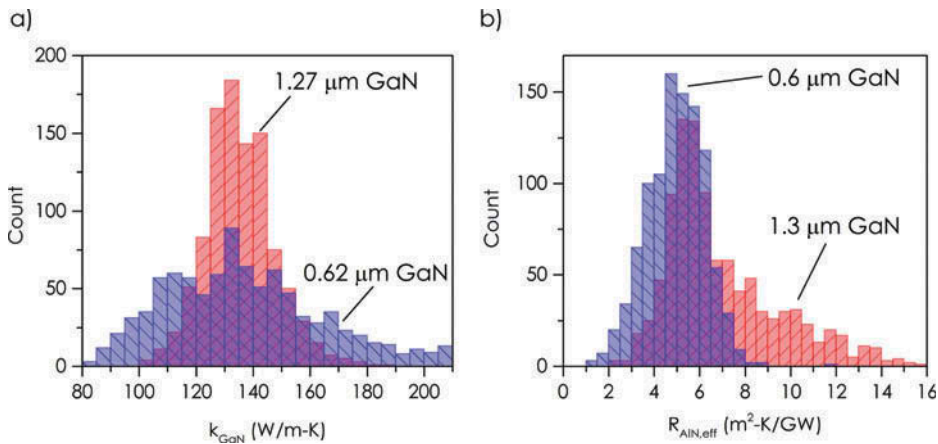


**Figure 6.** Comparison of histogram of best-fit values from Monte Carlo simulation for 1.3- $\mu\text{m}$  GaN and 0.6- $\mu\text{m}$  GaN (both on AlN/Si). (a) GaN thermal conductivity and (b) effective AlN resistance.

more accurately than that in the 1.3- $\mu\text{m}$  GaN sample. In each case more information can be gained by running the Monte Carlo simulation compared to estimating the uncertainty using the analytical equation.

## Conclusion

A number of different GaN on Si samples were tested and the thermal conductivity of these samples was not found to be heavily dependent upon thickness within the range of 0.3 to 1.3  $\mu\text{m}$ . The thermal conductivity of the thickest sample was  $136 \pm 19/14$  W/m-K. The effective resistance of the AlN transition layer between the GaN and Si was relatively low, between 7.0 and 5.3  $\text{m}^2\text{-K/GW}$  and appears to decrease slightly as the GaN thickness increases. The thermal resistance of the superlattice is nearly 10 times higher compared to a similar GaN on AlN structure, so the optimal configuration will have to weigh residual stress reduction with peak device temperature.

Directly simulating the uncertainty in TDTR measurements using a Monte Carlo method was demonstrated to provide greater accuracy compared to the analytical expression for parameters with low sensitivity, whereas the two methods agree well for parameters with high sensitivity. The increased complexity and computation time associated with the Monte Carlo simulation make the analytical expression advantageous for high-sensitivity parameters where accuracy is preserved.

## Acknowledgments

We thank Thomas Beechem for comparing our samples on his TDTR system and for helpful discussions.

## Funding

This work was supported by the National Science Foundation under IGERT award # DGE-1069138. Materials used in this study were provided by IQE.

## References

1. A. Dadgar, T. Hempel, J. Bläsing, O. Schulz, S. Fritze, J. Christen, and A. Krost, Improving GaN-on-Silicon Properties for GaN Device Epitaxy, *Physica Status Solidi C*, 8(5), 1503–1508, 2011.

2. D. G. Cahill, P. V. Braun, G. Chen, D. R. Clarke, S. Fan, K. E. Goodson, P. Keblinski, W. P. King, G. D. Mahan, and A. Majumdar, Nanoscale Thermal Transport. II. 2003–2012, *Applied Physics Reviews*, 1(1), 011305, 2014.
3. R. R. Reeber and K. Wang, Lattice Parameters and Thermal Expansion of GaN, *Journal of Materials Research*, 15(1), 40–44, 2000.
4. S. Nakanishi and T. Horiguchi, Surface Lattice Constants of Si (111), Ni (111) and Cu (111), *Japanese Journal of Applied Physics*, 20(3), L214–L216, 1981.
5. G. T. Hohensee, W. P. Hsieh, M. D. Losego, and D. G. Cahill, Interpreting Picosecond Acoustics in the Case of Low Interface Stiffness, *Review of Scientific Instruments*, 83(11), 114902–114906, 2012. doi:10.1063/1.4766957
6. D. G. Cahill, Analysis of Heat Flow in Layered Structures for Time-Domain Thermoreflectance, *Review of Scientific Instruments*, 75(12), 5119–5122, 2004.
7. A. J. Schmidt, X. Y. Chen, and G. Chen, Pulse Accumulation, Radial Heat Conduction, and Anisotropic Thermal Conductivity in Pump-Probe Transient Thermoreflectance, *Review of Scientific Instruments*, 79(11), 114902–114911, 2008. doi:10.1063/1.3006335
8. A. Schmidt, M. Chiesa, X. Y. Chen, and G. Chen, An Optical Pump-Probe Technique for Measuring the Thermal Conductivity of Liquids, *Review of Scientific Instruments*, 79(6), 064902–064907, 2008. doi:10.1063/1.2937458
9. A. J. Schmidt, *Optical Characterization of Thermal Transport from the Nanoscale to the Macroscale*, Boston, MA: Massachusetts Institute of Technology, 2008.
10. J. Liu, J. Zhu, M. Tian, X. Gu, A. Schmidt, and R. Yang, Simultaneous Measurement of Thermal Conductivity and Heat Capacity of Bulk and Thin Film Materials Using Frequency-Dependent Transient Thermoreflectance Method, *Review of Scientific Instruments*, 84(3), 034902, 2013.
11. D. G. Cahill and F. Watanabe, Thermal Conductivity of Isotopically Pure and Ge-Doped Si Epitaxial Layers from 300 to 550 K, *Physical Review B*, 70(23), 235322, 2004.
12. X. Wang, B. Cola, T. Bougher, S. Hodson, T. Fisher, and X. Xu, Photoacoustic Technique for Thermal Conductivity and Thermal Interface Measurements, in G. Chen, V. Prasad, and Y. Jaluria (eds.), *Annual Review of Heat Transfer*, 135–157, Redding, CT: Begell, 2013.
13. C. D. Wei, X. Zheng, D. G. Cahill, and J. C. Zhao, Invited Article: Micron Resolution Spatially Resolved Measurement of Heat Capacity Using Dual-Frequency Time-Domain Thermoreflectance, *Review of Scientific Instruments*, 84(7), 07130–07139, 2013. doi:10.1063/1.4815867
14. W. Jang, Z. Chen, W. Bao, C. N. Lau, and C. Dames, Thickness-Dependent Thermal Conductivity of Encased Graphene and Ultrathin Graphite, *Nano Letters*, 10(10), 3909–3913, 2010.
15. D. R. Thompson, S. R. Rao, and B. A. Cola, A Stepped-Bar Apparatus for Thermal Resistance Measurements, *Journal of Electronic Packaging*, 135(4), 041002, 2013.
16. C. E. Papadopoulos and H. Yeung, Uncertainty Estimation and Monte Carlo Simulation Method, *Flow Measurement and Instrumentation*, 12(4), 291–298, 2001.
17. Y. K. Koh, Y. Cao, D. G. Cahill, and D. Jena, Heat-Transport Mechanisms in Superlattices, *Advanced Functional Materials*, 19(4), 610615, 2009.
18. A. S. Glen, J. S. Leo, M. Donald, and A. F. Jaime, Some Effects of Oxygen Impurities on AlN and GaN, *Journal of Crystal Growth*, 246(3–4), 287298, 2002.
19. S. R. Choi, D. Kim, S.-H. Choa, S.-H. Lee, and J.-K. Kim, Thermal Conductivity of AlN and SiC Thin Films, *International Journal of Thermophysics*, 27(3), 896–905, 2006.
20. P. Kuo, G. Auner, and Z. Wu, Microstructure and Thermal Conductivity of Epitaxial AlN Thin Films, *Thin Solid Films*, 253(1), 223–227, 1994.
21. Y. Zhao, C. Zhu, S. Wang, J. Tian, D. Yang, C. Chen, H. Cheng, and P. Hing, Pulsed Photothermal Reflectance Measurement of the Thermal Conductivity of Sputtered Aluminum Nitride Thin Films, *Journal of Applied Physics*, 96(8), 4563–4568, 2004.
22. S. Zonghui, P. F. Justin, H. L. Jacob, A. P. Edward, F. D. Robert, and A. M. Jonathan, The Impact of Film Thickness and Substrate Surface Roughness on the Thermal Resistance of Aluminum Nitride Nucleation Layers, *Journal of Applied Physics*, 113(21), 213502, 2013.
23. B. F. Donovan, C. J. Szejewski, J. C. Duda, R. Cheaito, J. T. Gaskins, C.-Y. P. Yang, C. Constantin, R. E. Jones, and P. E. Hopkins, Thermal Boundary Conductance across Metal-Gallium Nitride Interfaces from 80 to 450 K, *Applied Physics Letters*, 105(20), 203502, 2014.
24. J. Cho, Y. Li, W. E. Hoke, D. H. Altman, M. Ashegi, and K. E. Goodson, Phonon Scattering in Strained Transition Layers for GaN Heteroepitaxy, *Physical Review B*, 89(11), 115301–115312, 2014. doi:10.1103/PhysRevB.89.115301
25. J. Liu, J. Zhu, M. Tian, X. K. Gu, A. Schmidt, and R. G. Yang, Simultaneous Measurement of Thermal Conductivity and Heat Capacity of Bulk and Thin Film Materials Using Frequency-Dependent Transient Thermoreflectance Method, *Review of Scientific Instruments*, 84(3), 034902–034914, 2013. doi:10.1063/1.4797479

26. C.-Y. Luo, H. Marchand, D. Clarke, and S. DenBaars, Thermal Conductivity of Lateral Epitaxial Overgrown GaN Films, *Applied Physics Letters*, 75(26), 4151–4153, 1999.
27. N. Killat, M. Montes, J. Pomeroy, T. Paskova, K. Evans, J. Leach, X. Li, Ü. Özgür, H. Morkoc, and K. Chabak, Thermal Properties of AlGa<sub>N</sub>/Ga<sub>N</sub> HFETs on Bulk Ga<sub>N</sub> Substrates, *IEEE Electron Device Letters*, 33(3), 366–368, 2012.
28. A. Sarua, H. Ji, K. P. Hilton, D. J. Wallis, M. J. Uren, T. Martin, and M. Kuball, Thermal Boundary Resistance between Ga<sub>N</sub> and Substrate in AlGa<sub>N</sub>/Ga<sub>N</sub> Electronic Devices, *IEEE Transactions on Electronic Devices*, 54(12), 31523158, 2007.
29. K. Gordiz and A. Henry, Examining the Effects of Stiffness and Mass Difference on the Thermal Interface Conductance between Lennard-Jones Solids, *Scientific Reports*, 5, 18361–18370, 2015. doi:[10.1038/srep18361](https://doi.org/10.1038/srep18361)
30. A. Manoi, J. W. Pomeroy, N. Killat, and M. Kuball, Benchmarking of Thermal Boundary Resistance in AlGa<sub>N</sub>/Ga<sub>N</sub> HEMTs on SiC Substrates: Implications of the Nucleation Layer Microstructure, *IEEE Electron Device Letters*, 31(12), 1395–1397, 2010.